Clemastine Induces an Impairment in Developmental Myelination

Ana Palma[1,2], Juan Carlos Chara[1,2], Alejandro Montilla[1,2], Amaia Otxoa-de-Amezaga[1], Francisca Ruíz-Jaén[3], Anna M. Planas[3], Carlos Matute[1,2], Alberto Pérez-Samartín[1,2] and María Domercq[1,2]*

[1]Achucarro Basque Center for Neuroscience and Department of Neurosciences, University of the Basque Country UPV/EHU, Leioa, Spain, [2]Centro de Investigación Biomédica en Red de Enfermedades Neurodegenerativas (CIBERNED), Leioa, Spain, [3]Department of Neuroscience and Experimental Therapeutics, Institute for Biomedical Research of Barcelona (IIBB), Spanish National Research Council (CSIC), Institut d'Investigacions Biomèdiques August Pi i Sunyer (IDIBAPS), Barcelona, Spain

Abnormalities in myelination are associated to behavioral and cognitive dysfunction in neurodevelopmental psychiatric disorders. Thus, therapies to promote or accelerate myelination could potentially ameliorate symptoms in autism. Clemastine, a histamine H1 antagonist with anticholinergic properties against muscarinic M1 receptor, is the most promising drug with promyelinating properties. Clemastine penetrates the blood brain barrier efficiently and promotes remyelination in different animal models of neurodegeneration including multiple sclerosis, ischemia and Alzheimer's disease. However, its role in myelination during development is unknown. We showed that clemastine treatment during development increased oligodendrocyte differentiation in both white and gray matter. However, despite the increase in the number of oligodendrocytes, conduction velocity of myelinated fibers of *corpus callosum* decreased in clemastine treated mice. Confocal and electron microscopy showed a reduction in the number of myelinated axons and nodes of Ranvier and a reduction of myelin thickness in *corpus callosum*. To understand the mechanisms leading to myelin formation impairment in the presence of an excess of myelinating oligodendrocytes, we focused on microglial cells that also express muscarinic M1 receptors. Importantly, the population of CD11c^{+} microglia cells, necessary for myelination, as well as the levels of insulin growth factor-1 decrease in clemastine-treated mice. Altogether, these data suggest that clemastine impact on myelin development is more complex than previously thought and could be dependent on microglia-oligodendrocyte crosstalk. Further studies are needed to clarify the role of microglia cells on developmental myelination.

Keywords: clemastine, myelin, oligodendrocyte, microglia, development

INTRODUCTION

Myelin directs node of Ranvier formation, enables rapid saltatory conduction, communicates with axons *via* the periaxonal space and provides metabolic support to them. Myelin, as other structures in brain, is subject to plastic changes in response to electrical activity that allow to fine tune circuits involved in motor learning and memory (McKenzie et al., 2014). Changes in the number or structure of myelin sheaths, nodes of Ranvier and periaxonal space modulate axon conduction velocity. Myelin formation includes diverse and very controlled events: migration and proliferation of

oligodendrocyte progenitor cells (OPCs), recognition of target axons, differentiation of OPCs into mature oligodendrocytes, membrane outgrowth, axonal wrapping, and myelin compaction. Myelination takes place during the developmental critical period of plasticity, when experience can rapidly change cortical structure and function. Moreover, early GABAergic communication between OPCs and interneurons determines interneuron maturation and myelination (Fang et al., 2021). Thus, myelination could have a more active role in circuit refinement and maturation during development. The importance of myelin for circuit function is made apparent by the severity of neurological diseases associated with its disruption. Abnormalities in myelination during development cause cognitive dysfunction and are associated to behavioral disturbances in neurodevelopmental psychiatric disorders, as reported in several animal models of syndromic Autism Spectrum Disorders (ASD). For instance, the normal process of myelination is delayed in contactin-associated protein-like 2 (caspr2) knock out mice (Scott et al., 2019); besides, a mouse model of Pitt–Hopkins syndrome (PTHS), a syndromic form of ASD, showed reductions in mature oligodendrocyte numbers and myelination (Phan et al., 2020). However, to date, there is no therapy to compensate or alleviate neurodevelopmental abnormalities or delays of myelination. The fact that myelin is transiently altered in these neurodevelopmental disorders point to pro-myelinating drugs as a promising therapeutic approach.

Oligodendrocytes myelinate CNS axons following an innate but precisely regulated and orchestrated process to achieve the correct amount of myelinated axons. The main external cue controlling myelination is the axons, which provide physical and chemical signals to guide oligodendroglial processes in axonal myelin wrapping. Oligodendrocytes interact not only with axons, but also with the extracellular matrix (ECM) and glial cells. The ECM mediates the integration of growth factors and regulates cytoskeletal dynamics (Lau et al., 2013). Recent findings suggest that microglia are also involved in myelination by supporting oligodendrogenesis and myelinogenesis as well as by remodeling myelin and removing abnormal myelin through phagocytosis (excellently reviewed in Santos and Fields, 2021). Microglia have a high phagocytic activity during early postnatal development (Li et al., 2019) and are able to engulf myelin sheaths to sculpt myelination according to axonal activity (Hughes and Appel, 2019; Li et al., 2019), to phagocytose living NG2+ OPCs (Nemes-Baran et al., 2020) and to remove myelin abnormalities during development (Djannatian et al., 2021). In addition, microglia also support oligodendroglia survival and maturation through the release of growth factors (Li et al., 2019). Importantly, a particular CD11c+ microglia subset that predominates in primary myelinating areas of the developing brain is essential for myelinogenesis (Wlodarczyk et al., 2017). These cells are the main source of insulin growth factor (IGF) (Wlodarczyk et al., 2017) which is essential for myelination. These new data highlight the importance of microglia in remodeling myelination, maintaining a balanced oligodendroglial population and promoting myelinogenesis.

Clemastine is to date the most promising pro-myelinating drug. Clemastine is an antihistaminic compound with anti-

muscarinic properties against the muscarinic receptor 1 (M1R) (de Angelis et al., 2012). Previous reports confirm that muscarinic M1 receptors are expressed by oligodendroglial cells and may modulate OPC proliferation and differentiation (de Angelis et al., 2012; Deshmukh et al., 2013; Mei et al., 2014). Moreover, M1Rs antagonist clemastine, as well as other antagonists such as benztropine, promote remyelination in animal models of multiple sclerosis (Deshmukh et al., 2013; Mei et al., 2014), after hypoxia (Cree et al., 2018; Wang et al., 2018) and prevent demyelination secondary to aging and in Alzheimer's disease (Wang et al., 2020; Chen et al., 2021). However, little is known about the effect of clemastine in the absence of myelin abnormalities or demyelination. Here, we analyzed the impact of clemastine in myelination during development. Surprisingly, clemastine decreased axon conduction velocity despite the increase in oligodendrogenesis. Our data point to microglia as another target of clemastine involved in developmental myelination.

MATERIALS AND METHODS

Animal Treatments
Experiments were performed in C57BL/6 wild-type mice and CD11c+ eYFP mice (generously provided by the Laboratory of Cerebrovascular Research, IIBB-CSIC, Barcelona). All experiments were performed according to the procedures approved by the Ethics Committee of the University of the Basque Country (UPV/EHU). Animals were handled in accordance with the European Communities Council Directive. Animals were kept under conventional housing conditions (22 ± 2°C, 55 ± 10% humidity, 12-hour day/night cycle and with *ad libitum* access to food and water) at the University of the Basque Country animal unit. All possible efforts were made to minimize animal suffering and the number of animals used. C57BL/6 wild-type mice were daily treated with vehicle or clemastine (#1453 Tocris; 50 mg/kg solved in 10% DMSO) by intraperitoneal injections from postnatal day 5 (P5) to P21. CD11c+ eYFP mice were treated from P5 to P10 following the same protocol.

Immunohistochemistry
Mice were transcardially perfused with 4% p-formaldehyde (PFA) in 0.1 M sodium phosphate buffer (PBS) (pH 7.4) and post-fixated in 4% PFA for 4 h. Tissue was cut using a Microm HM650V vibratome (40 μm). After blocking with 4% normal goat serum in PBS plus 0.1% Triton X-100 (blocking solution) for 1 h at room temperature, free-floating sections were incubated with primary antibodies overnight at 4°C in blocking solution. The following antibodies were used: anti-APC (1: 500 #OP80 Sigma), anti-Olig2 (1:1000 #MABN50 Sigma), anti-caspr (1:500 #MABN69 Sigma), anti-MBP (1:1000 #808401 Biolegend), anti-Nav1.6 (1:500 #ASC-009 Alomone), anti-iNOS (1:500 #610329 BDBiosciences), anti-PDGFRα (1:250 #sc-398206 SantaCruz Biotechnology), anti-Iba1 (1:500 #019-19741 Wako), anti-P2Y12 (1:200 #AS-55043A AnaSpec), anti-MRC1 (1:2000 #ab64693 Abcam), anti-Ki-67 (1:500 #VP-RM04 Vector

Laboratories), anti-cleaved caspase 3 (1:400 #9661 Cell Signaling) and anti-GFAP (1:50 #MAB3402 Sigma). Tissue sections were washed and incubated with the appropriate secondary antibodies: AlexaFluor-488, -594, and -647 anti-rat, anti-rabbit, anti-guinea pig, and anti-mouse IgG secondary antibodies (Invitrogen) for 1 h at room temperature. Cell *nuclei* were stained using DAPI (1: 1000 Vector Laboratories).

Images were acquired with the same settings for all samples within one experimental group. Zeiss LSM800, Zeiss LSM880 Airyscan and Leica TCS SP8 confocal microscope were used to acquire the images. To quantify the differentiation of oligodendrocytes, z-stack images (40X) were taken using a Leica TCS SP8 confocal microscope. Results were expressed as a percentage of APC$^+$ and PDGFR$^+$ *vs* the total number of Olig2$^+$ oligodendrocytes. Oligodendroglial proliferation and cell death was quantified using Ki67 and Casp-3 immunostaining respectively and results were normalized to area. To quantify the number and length of nodes of Ranvier and paranodes in *corpus callosum* and cerebral cortex, high magnification (×63) z-stack images were taken using a Zeiss LSM800 confocal microscope and analysis was performed in maximal projections obtained with ImageJ software (NIH). Node and paranodes length were only measured when a node and its flanking paranodes were completely defined using antibodies to caspr and Na$_v$1.6. To measure internode length in cerebral cortex, high magnification (×40) z-stack images were taken using a Zeiss LSM800 confocal microscope. Individual internodes were traced as MBP$^+$ processes flanked by caspr$^+$ paranodes and the length analyzed using ImageJ software. To quantify microglia Iba1, CD68 and iNOS expression, high magnification (×63) images were taken using a Leica TCS SP8 super resolution microscope. Immunoreactivity of Iba1 and iNOS was determined by applying default threshold with the ImageJ software and was normalized to area. CD68$^+$ *puncta* were quantified and normalized to the number of cells. To quantify the number of microglial cells phagocytosing MBP$^+$ myelin and/ or olig2$^+$ cells, high magnification (×40) z-stacks images were taken using a Zeiss LSM800 confocal microscopy. Results were normalized to the number of cells and expressed in percentage. Analysis was performed in at least three different sections of $n =$ 4–6 mice. To analyze the morphology of Iba1$^+$ microglia from cerebral cortex, high magnification (×63) z-stack images were taken with Zeiss LSM800 confocal microscope. Individual microglia cell was firstly skeletonized to perform Sholl analysis (ImageJ plugin) as well as branches and junctions quantifications (at least 20–25 cells *per* mice). In all cases, data come from $n = 6$ mice *per* group from two different litters.

Electron Microscopy

Mice were perfused with 4% p-formaldehyde, 2.5% glutaraldehyde and 0.5% NaCl in phosphate buffer, pH7.4. The brains were postfixed with the same fixative solution overnight at 4°C. The tissue was sagittally cut using a Leica VT 1200S vibrating blade microtome (Leica microsystems) to obtain 200 μm-thick sections. Tissue sections were postfixed in 2% OsO4, dehydrated in ethanol and propylenoxide, and embedded in EPON (Serva) for 24 h at 60°C. Ultrathin 50 nm

sections were obtained using a Leica Ultracut S ultramicrotome (Leica) and contrasted with 4% uranyl acetate (30 min) and lead citrate (6 min). High resolution electron microscope images were taken using a Zeiss EM900 electron microscope (Zeiss). Sectioning, imaging and analysis were carried out by an experimenter blind to the treatment group. Image analysis was performed using ImageJ (NIH). The g-ratio of myelinated axons was calculated as the ratio of the inner to the outer *radius* of the myelin sheath using ×8,000 magnification images from at least 100–150 axons from 60 images *per* animal. The number of myelinated axons was quantified using ×1,000 magnification images.

Microglia Culture

Primary mixed glial cultures were prepared from the cerebral cortex of neonatal rats and mice (P0–P2). After 10–15 days in culture, microglia were isolated by mechanical shaking (400 rpm, 1 h) and cultured as previously described (Domercq et al., 2007).

Myelin Phagocytosis Assay

Mouse myelin was isolated as previously described (Norton & Poduslo, 1973). Briefly, brain was mechanically homogenized in 0.32 M sucrose and subjected to repeated sucrose gradient centrifugation and osmotic shocks to separate myelin from other cellular components. Myelin was incubated with Alexa488-NHS dye (A2000 Life Technologies) for 1 h 45 min at RT in PBS (pH 8). Dyed myelin was dialyzed for removing dye excess, resuspended in PBS (pH 7.4), vortexed for 60 s for fragmentation in homogeneous size aggregates and added to microglia culture medium (1:200 dilution). Microglia was rinsed and fixed after being exposed to myelin for 1 h at 37°C; subsequently, myelin accumulation was calculated measuring the positive area in individual cells. Myelin endocytosis *per* cell was quantified in at least 10-20 cells *per* coverslip from $n = 3$ independent experiments performed in duplicate.

Cytosolic Ca^{2+} Imaging

To measure cytosolic [Ca^{2+}], cells were loaded with Fluo-4 AM (1 mM; Molecular Probes, Invitrogen) in incubation buffer for 30 min at 37°C and washed (20 min). Images were acquired through a ×63 objective by an inverted LCS SP8 confocal microscope (Leica, Germany) at an acquisition rate of 1 frame/15 s during 5 min. For data analysis, a homogeneous population of 15–25 cells was selected in the field of view and cell *somata* selected as ROIs. Background values were always subtracted and data was expressed as F/F0 ± s.e.m. (%) in which F represents the fluorescence value for a given time point and F0 represents the mean of the resting fluorescence level.

Microglia Sorting and qPCR Analysis

Total brain was homogenated and digested mechanically and enzymatically, and myelin debris was removed through a continuous ×60 percoll gradient. Microglia was sorted using CD11b (#101205, 1:100; Biolegend) and CD45 (#103134, 1: 100; Biolegend), to distinguish between resident microglia (CD11b$^+$/CD45^{low}) and macrophages (CD11b$^+$/CD45^{high}; Szulzewsky et al., 2015). Microglia was directly collected in

Target gene	Forward (5′->3′)	Reverse (5′->3′)
Itgax	GAACATATCCCTGGGCCTGTC	CACAGTAGGACCACAAGCCAA
Spp1	GCTTTTGCCTGTTTGGCATT	AATCAGTCACTTTCACCGGGAG
ApoE	AGGTCCAGGAAGAGCTGCAG	GTGCCGTCAGTTCTTGTGTGA
IGF-1	AGAAGTCCCCGTCCCTATCG	CCTTCTCCTTTGCAGCTTCG
CD68	CAAGCCCAAATTCAAATCCG	CCAAGCCTTTCTTCCACCC
H2-Ab1	AGGGCGGAGACTCCGAAA	GAAGTAGCACTCGCCCATGAAC
Arg1	GGATTGGCAAGGTGATGGAA	CGACATCAAAGCTCAGGTGAA
Bdnf	TCCAAAGGCCAACTGAAGCA	CTGCAGCCTTCCTTGGTGTA
C3	AGGGAGTGTTTGTGCTGAAC	GCCAATGTCTGCCTTCTCTAC
Ccl2	AGCAGCAGGTGTCCCAAA	TTCTTGGGGGTCAGCACAGAC
Cd36	GGTGTGCTAGACATTGGCAAA	GACTTGCATGTAGGAAATGTGGAA
Cd86	CATGGGCTTGGCAATCCTTA	ATTGAAATAAGCTTGCGTCTCC
Chi3l3	GCCCACCAGGAAAGTACACA	CCTCAGTGGCTCCTTCATTCA
Clec7a	ACCACAAGCCCACAGAATCA	AGGAAGGCAAGGCTGAGAAA
Mrc1	CACAAAGCCATGCTGTAGTACC	GTAAAACCCATGCCGTTTCCA
Nos2	GAGGAGCAGGTGGAAGACTA	GGAAAAGACTGCACCGAAGATA
P2ry12	GATGCCAGTCTGCAAGTTCC	TTGACACCAGGCACATCCA
Trem2	ACCTCTCCACCAGTTTCTCC	AGTACATGACACCCTCAAGGAC
Tyrobp	GCTGAGACTGAGTCGCCTTA	CTCTGTGTGTTGAGGTCACTGTA

RNA lysis buffer and total RNA was extracted using the RNeasy Plus Micro Kit (#74034) (Quiagen). RNA concentration and integrity were analyzed with the collaboration of the General Genomics Service Sequencing and Genotyping Unit from the UPV/EHU. A battery of microglia genes (**Table 1**) associated to microglia DAM signature, inflammatory reaction and/or phagocytosis was analyzed. Gene expression was analyzed using a 96.96 Dynamic Array™ integrated fluidic circuit (Fluidigm) real-time PCR and GenEx software. Results were depicted as relative gene expression according to the ΔΔCq method (2−ΔΔCt) and expressed in base 2 logarithmic scale.

Electrophysiology

Mice were anesthetized and decapitated and the brain was rapidly removed and placed in ice-cold (4°C) cutting artificial cerebrospinal fluid (ACSF) containing (in mM): 215 Sucrose, 2.5 KCl, 26 NaHCO3, 1.6 NaH2PO4, 20 Glucose, 1 CaCl2, 4 MgCl2, and 4 MgSO4 bubbled with a mixture of 95% O2/5% CO2. Coronal slices, 400-μm thick, were cut on a Leica VT1200S vibratome and transferred to a warmed (~36°C) solution of normal ACSF (nACSF) containing (in mM): 124 NaCl, 2.5 KCl, 10 glucose, 25 NaHCO3, 1.25 NaH2PO4, 2.5 CaCl2, and 1.3 MgCl2 for recovery (45 min). Compound action potentials (CAPs) were evoked by electrical stimulation of the *corpus callosum* with a bipolar electrode (CE2C55, FHC) and were recorded with a pulled borosilicate glass pipette (1.6 MΩ resistance) filled with NaCl 3 M within the contralateral *corpus callosum*. Stimulation intensities ranged from 30 to 3000 μA (100 μs pulses, Master-8, AMPI). Input-output curves were generated by recording the amplitudes of myelinated N1 and partially myelinated fibers N2 as a function of stimulation intensity. Conduction velocity values for N1 and N2 fibers were calculated as the slope of a straight line fitted through a plot of the distance between the recording and stimulating electrodes *versus* the response latency (time to N1 and N2 respectively). Recordings were performed at 4 different distances from the recording electrode (500, 1000, 1500 and 2000 μm). Three responses were averaged for each measurement. Peak amplitudes and latencies were calculated using custom written routines in pCLAMP 10.0 (Molecular Devices).

Statistical Analysis

Data are presented as mean ± s.e.m. with sample size and number of repeats indicated in the figure legends. Statistical analysis was performed using GraphPad Prism statistical software (version 7.0; GraphPad software). Comparisons between two groups were analysed using paired Student's two-tailed t-test. Statistical significance was considered at $p < 0.05$.

RESULTS

Clemastine Increases the Number of Mature Oligodendrocytes in Developing Brain

To determine whether clemastine treatment *in vivo* promotes myelination during development, we treated mice with clemastine (50 mg/kg/day, i.p.) or vehicle from postnatal day 5–20, a time window coincident with myelination and within the critical period of brain plasticity (**Figure 1A**). We first quantified the population of oligodendrocyte progenitor cells (OPCs) and mature oligodendrocytes (OLs) using antibodies against PDGFRa and CC1 (anti-APC), respectively. We performed blinded cell counts in three different areas, *corpus callosum* (CC), retrosplenial cortex (Rsp Ctx) and somatosensory cortex (SSp Ctx), on anatomically equivalent brain sections and normalized our counts using the pan-OL marker Olig2. As showed *in vitro* (Mei et al., 2014, 2016), clemastine induced a significant increase in the proportion of APC[+] OLs in *corpus callosum* as well as in cerebral cortex (**Figure 1B**). In parallel, we detected a decrease in
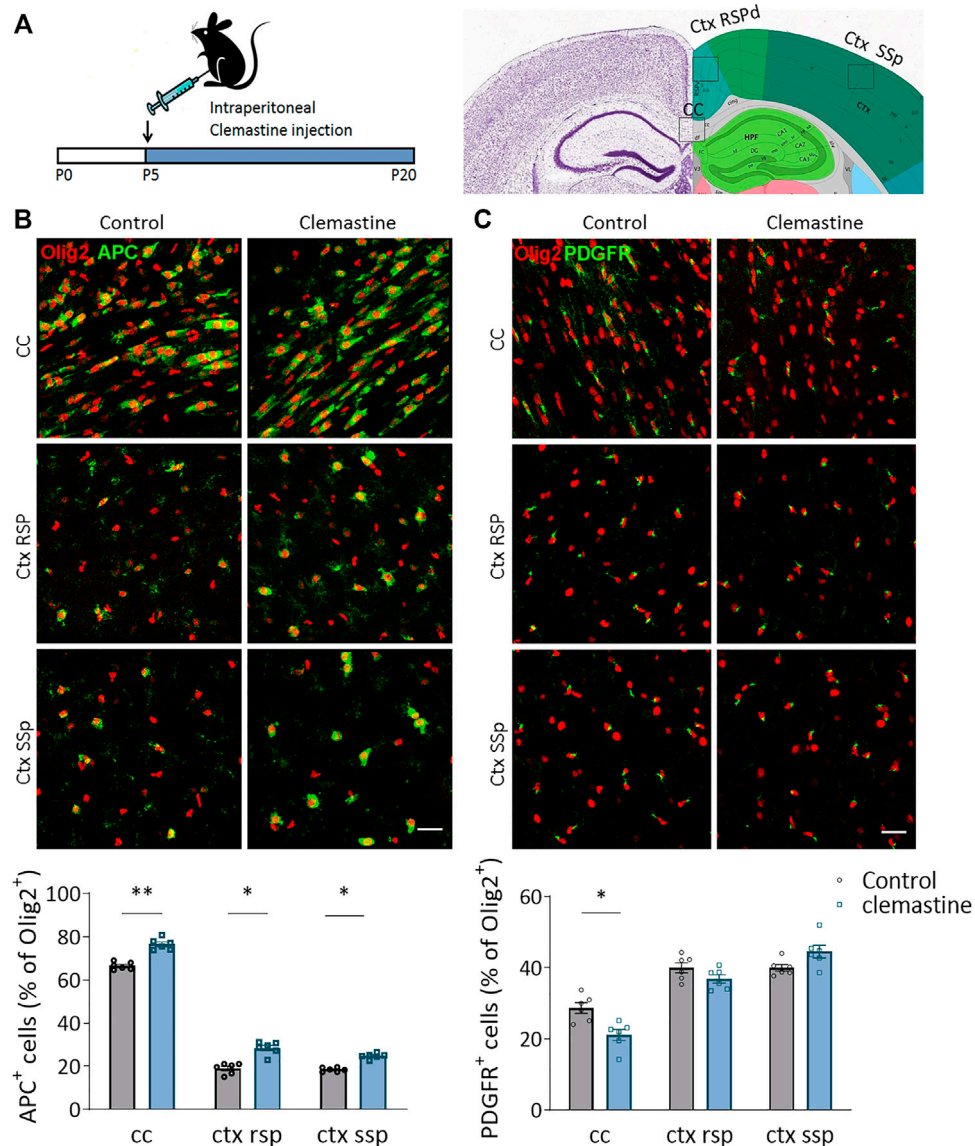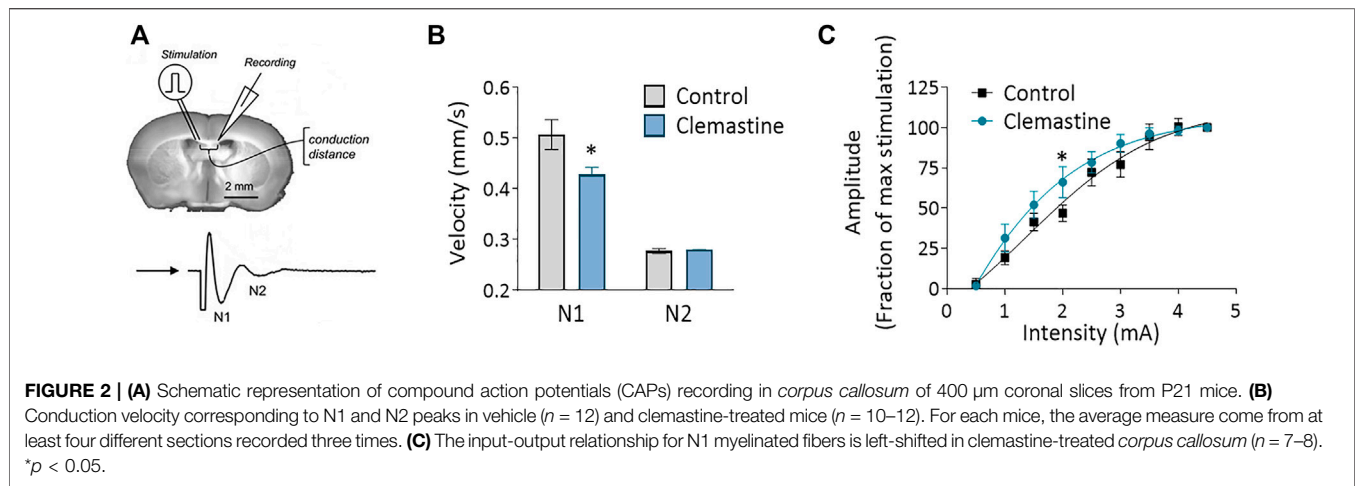
FIGURE 1 | (A) Schematic representation of clemastine treatment (50 μg/kg; i.p.) during development. The analysis was performed in *corpus callosum* (cc), retrospinal cortex (ctx rsp) and primary somatosensory cortex (ctx ss) at postnatal day 21 (P21). (B,C) Compressed confocal z stack images of APC$^+$ mature oligodendrocytes [(B); green] and PDGFR$^+$ oligodendrocyte progenitor cells [(C); OPCs; green] in cc, ctx rsp and ctx ss of control and clemastine-treated mice. Below, average of the percentage of mature oligodendrocytes (B) or OPCs (C) *vs* total Olig^{2+} oligodendroglial cells ($n = 6$ mice *per* experimental group). Scale bar = 50 μm *$p < 0.05$, **$p < 0.01$.

the proportion of PDGFR$^+$ OPCs in *corpus callosum*. In contrast, no change in the number of PDGFR$^+$ OPCs was detected in cerebral cortex (**Figure 1C**). We further analyzed the impact of clemastine on OPC proliferation and oligodendrocyte survival using antibodies to Ki67 and caspase-3, respectively. As expected, clemastine induced a decrease in the number of Ki67$^+$ Olig2$^+$ cells in *corpus callosum* and cerebral cortex, although only significant in cerebral cortex, suggesting that clemastine reduces OPC proliferation (**Supplementary Figure S1**). We did not observe any change in the number of casp-3$^+$ oligodendrocytes in *corpus callosum* (**Supplementary Figure S1**), excluding any effect of clemastine on oligodendrocyte survival. Practically no Olig2$^+$ cell

death was detected in cerebral cortex, and therefore, we excluded this region for the analysis. These results indicate that the treatment with clemastine during development promotes the maturation of the oligodendroglial lineage by increasing the percentage of APC$^+$ OLs, particularly in the *corpus callosum*.

Conduction Velocity of the Interhemispheric Fibers From *Corpus Callosum* Decreased After Clemastine Treatment

As clemastine induced a clear increase in OL differentiation in the *corpus callosum*, we hypothesized that this would translate into

FIGURE 2 | (A) Schematic representation of compound action potentials (CAPs) recording in *corpus callosum* of 400 µm coronal slices from P21 mice. **(B)** Conduction velocity corresponding to N1 and N2 peaks in vehicle ($n = 12$) and clemastine-treated mice ($n = 10$–12). For each mice, the average measure come from at least four different sections recorded three times. **(C)** The input-output relationship for N1 myelinated fibers is left-shifted in clemastine-treated *corpus callosum* ($n = 7$–8). *$p < 0.05$.

accelerated myelination and a subsequent increase in the conduction velocity in white matter. To test this idea, we measured the propagation of compound action potential (CAPs) in the *corpus callosum* by performing electrophysiological recordings in acute coronal brain slices. CAPs were evoked by a bipolar stimulating electrode and recorded by a field electrode placed at varying distances across the *corpus callosum*. Surprisingly, our results revealed that action potentials transmission was significantly slower in myelinated axons (N1) of clemastine treated mice compared to control mice (**Figure 2**, $p < 0.01$, $n = 10$–12). In contrast, the conduction velocity in unmyelinated axons (N2) is similar between groups (**Figure 2**, $n = 10$–12). Examining the relationship between stimulus intensity and response magnitude (input output curve) revealed that myelinated axons in clemastine-treated mice tended to be more excitable than those in control mice (**Figure 2C**). Therefore, we concluded that clemastine induced a delay in action potential propagation despite the effect in OL differentiation.

Clemastine Administration During Development Reduces the Number of Nodes of Ranvier and Myelinated Axons in *Corpus Callosum*
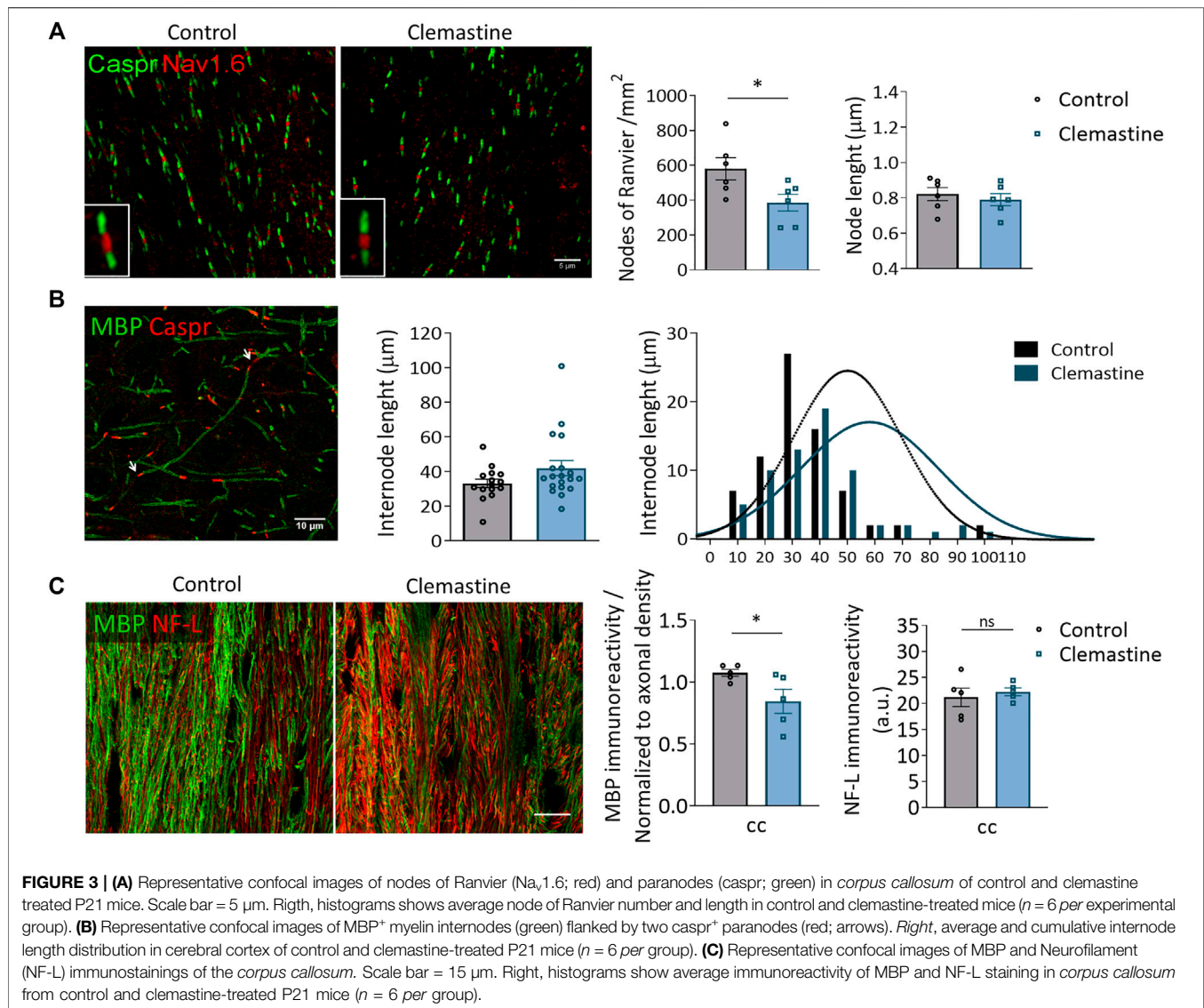
Since the increase in the percentage of mature OLs was not accompanied by an increase in the conduction velocity of N1 fibers in *corpus callosum*, myelination was further studied by performing histological analyses both by confocal and transmission electron microscopy. The speed of action potential conduction depends on the length and the number of the nodes of Ranvier (Arancibia-Cárcamo et al., 2017), in addition to myelin sheath number and structure, and node length is plastic and refined in response to electrical activity. We immunolabeled coronal brain sections with antibodies against contactin-associated protein (caspr) and sodium-gated channels 1.6 ($Na_v1.6$) to visualize paranodes and nodes of Ranvier respectively. By identifying regions of dense $Na_v1.6$ staining that were clearly flanked by abutting caspr[+] paranodes, we

quantified the length of individual nodes within *corpus callosum* in control and clemastine-treated mice. We did not find any change in node length (**Figure 3A**). However, we detected a significant reduction in the number of nodes of Ranvier in clemastine-treated mice (**Figure 3A**). We also measured the length of internodes that were flanked on each end by contactin-associated protein (caspr[+]) paranodes. We found that clemastine treatment tended to increase internode length, although the differences were not significant (**Figure 3B**). Confocal immunohistochemical analysis of sections immunolabeled with antibodies to myelin basic protein (MBP) revealed a small reduction in myelinated fibers in *corpus callosum* (**Figure 3C**) without affecting the density of axons (**Figure 3C**).

As the high density of myelin sheaths in *corpus callosum* made it difficult to look for differences using confocal microscopy, we further analyze myelination using transmission electron microscopy (TEM). TEM images were taken of the *corpus callosum* directly above the dorsal *hippocampus* from anatomically equivalent tissue sections from control and clemastine-treated mice. We observed that the number of myelinated axons, quantified by TEM, was reduced after clemastine treatment (**Figure 4A**). Myelin thickness was assessed by g-ratio calculation (axon diameter/total outer diameter of myelinated fiber). G-ratio analysis revealed thinner myelin sheaths in small caliber axons (0–0.5 µm) of treated animals (**Figure 4B**), while no differences were found in axons from 0.5 to 1 µm diameter, indicating that the changes observed in myelin thickness depend on axons diameter (**Figure 4B**). Taken together, our findings suggest that, although clemastine treatment during development initially enhances oligodendrocyte differentiation, functional myelination is impaired or delayed.

Clemastine Treatment Modifies the Expression of Activation Markers and the Morphology of Microglia in Developing Brain
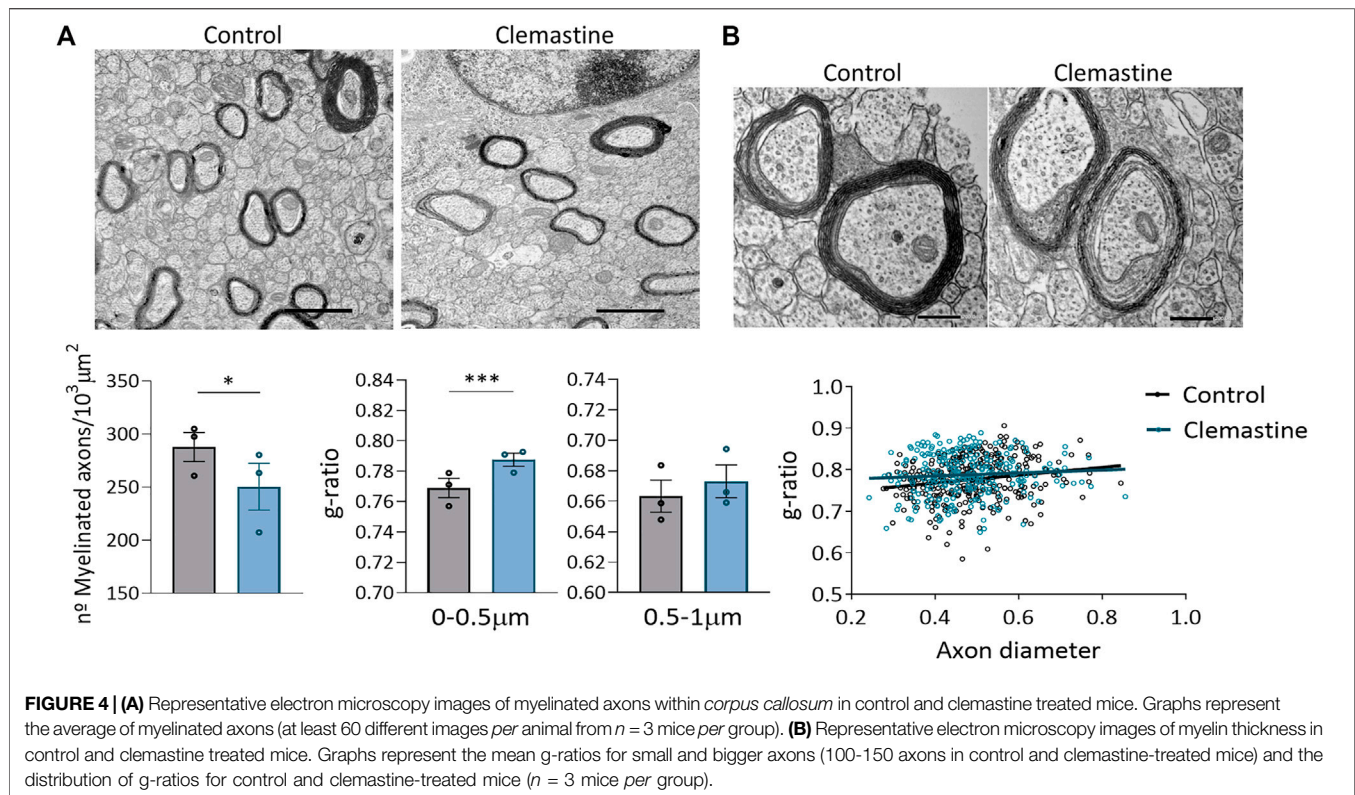
In addition to electrical activity, developmental myelination depends on the crosstalk with other glial cells, astrocytes

FIGURE 3 | (A) Representative confocal images of nodes of Ranvier (Na$_v$1.6; red) and paranodes (caspr; green) in *corpus callosum* of control and clemastine treated P21 mice. Scale bar = 5 µm. Rigth, histograms shows average node of Ranvier number and length in control and clemastine-treated mice (*n* = 6 *per* experimental group). **(B)** Representative confocal images of MBP$^+$ myelin internodes (green) flanked by two caspr$^+$ paranodes (red; arrows). *Right*, average and cumulative internode length distribution in cerebral cortex of control and clemastine-treated P21 mice (*n* = 6 *per* group). **(C)** Representative confocal images of MBP and Neurofilament (NF-L) immunostainings of the *corpus callosum.* Scale bar = 15 µm. Right, histograms show average immunoreactivity of MBP and NF-L staining in *corpus callosum* from control and clemastine-treated P21 mice (*n* = 6 *per* group).

(Dutta et al., 2019; Yalcin and Monje, 2021) and particularly microglial cells (Santos and Fields, 2021). Chmr1, the receptor mediating clemastine-effect in OLs, is also expressed in microglia, as reported from previous RNAseq analysis (**Figure 5A**; Zhang et al., 2014). Indeed, cultured microglia cells exposed to muscarine showed a significant increase in cytosolic *calcium*, as revealed with Fluo4- *calcium* imaging (**Figure 5B**). In contrast, astrocytes express low levels of the *Chmr1* gene and immunohistochemical analysis using antibodies to GFAP revealed no significant changes in astrocyte number or activation (**Supplementary Figure S2**). We hypothesized that the impairment in myelination during development could be related to the interaction of clemastine with microglial cells. So, we next analyzed by immunohistochemistry microglia morphology and activation markers. Clemastine treatment did not alter the number of microglial cells or the immunoreactivity of Iba1, indicating no change in microglia population. Additionally, we examined the morphology of Iba1+ microglia

from control and treated mice (**Figure 5C**). For that, we quantified the number of branches and junctions *per* cell, as well as, the cellular complexity as determined by Sholl analysis. Both data demonstrated an increase in the morphology complexity and ramification in microglia from clemastine-treated mice (**Figure 5D**). Since the activation state of microglia is determinant for the remyelination capacity of OPCs (Zabala et al., 2018), we wondered whether clemastine could alter microglia activation state. Clemastine induced a massive reduction in the expression of iNOS, a proinflammatory marker, as well as the expression of the phagocytic marker CD68 (**Figures 5E,F**). All these data suggest that clemastine modulates microglial shape and function during development.

We further explored the expression of pro-inflammatory/anti-inflammatory genes, lipid and phagocytosis markers as well as growth factors involved in developmental myelinogenesis and adaptive myelination (Geraghty et al., 2019; Wlodarczyk et al.,

FIGURE 4 | (A) Representative electron microscopy images of myelinated axons within *corpus callosum* in control and clemastine treated mice. Graphs represent the average of myelinated axons (at least 60 different images *per* animal from *n* = 3 mice *per* group). **(B)** Representative electron microscopy images of myelin thickness in control and clemastine treated mice. Graphs represent the mean g-ratios for small and bigger axons (100-150 axons in control and clemastine-treated mice) and the distribution of g-ratios for control and clemastine-treated mice (*n* = 3 mice *per* group).
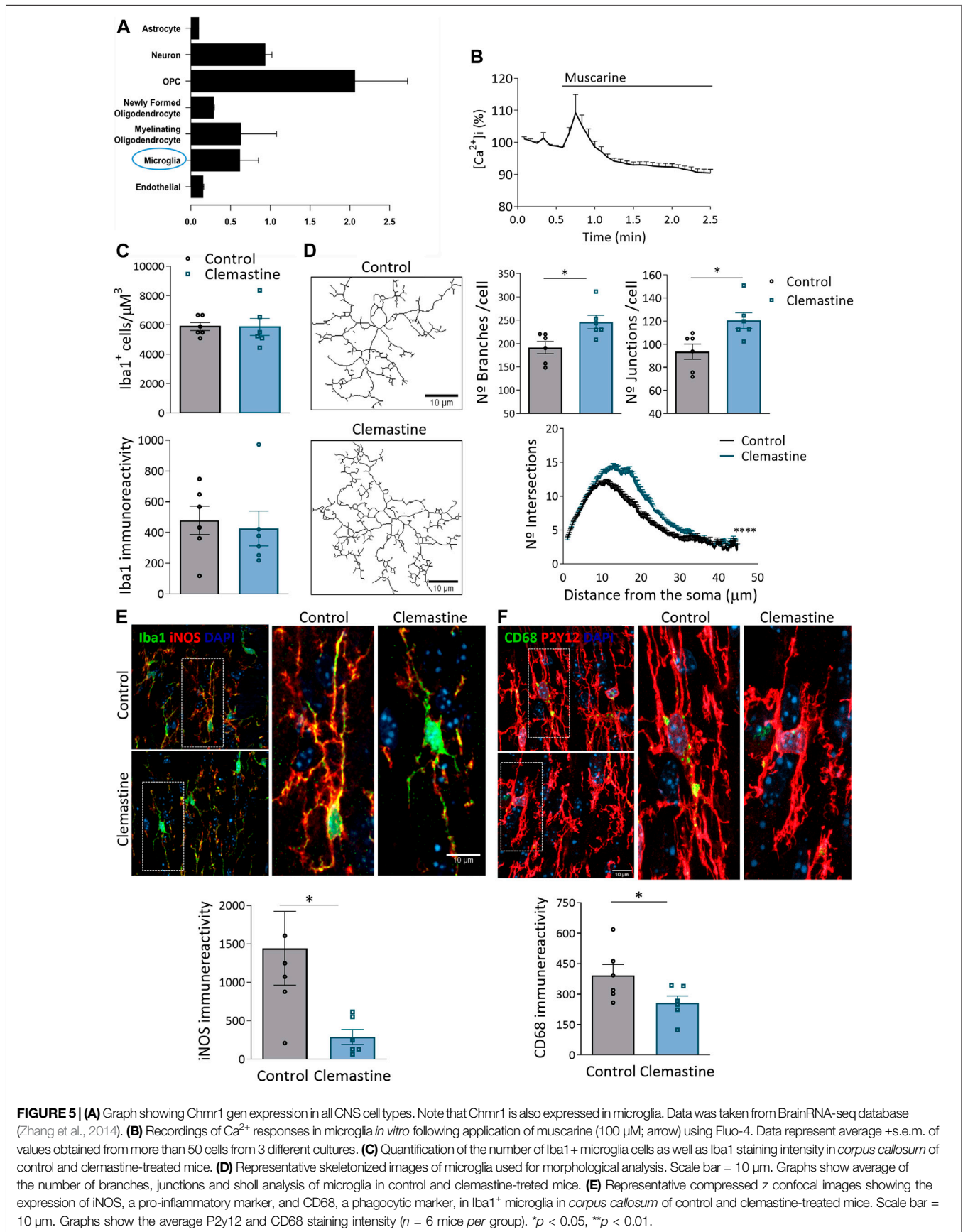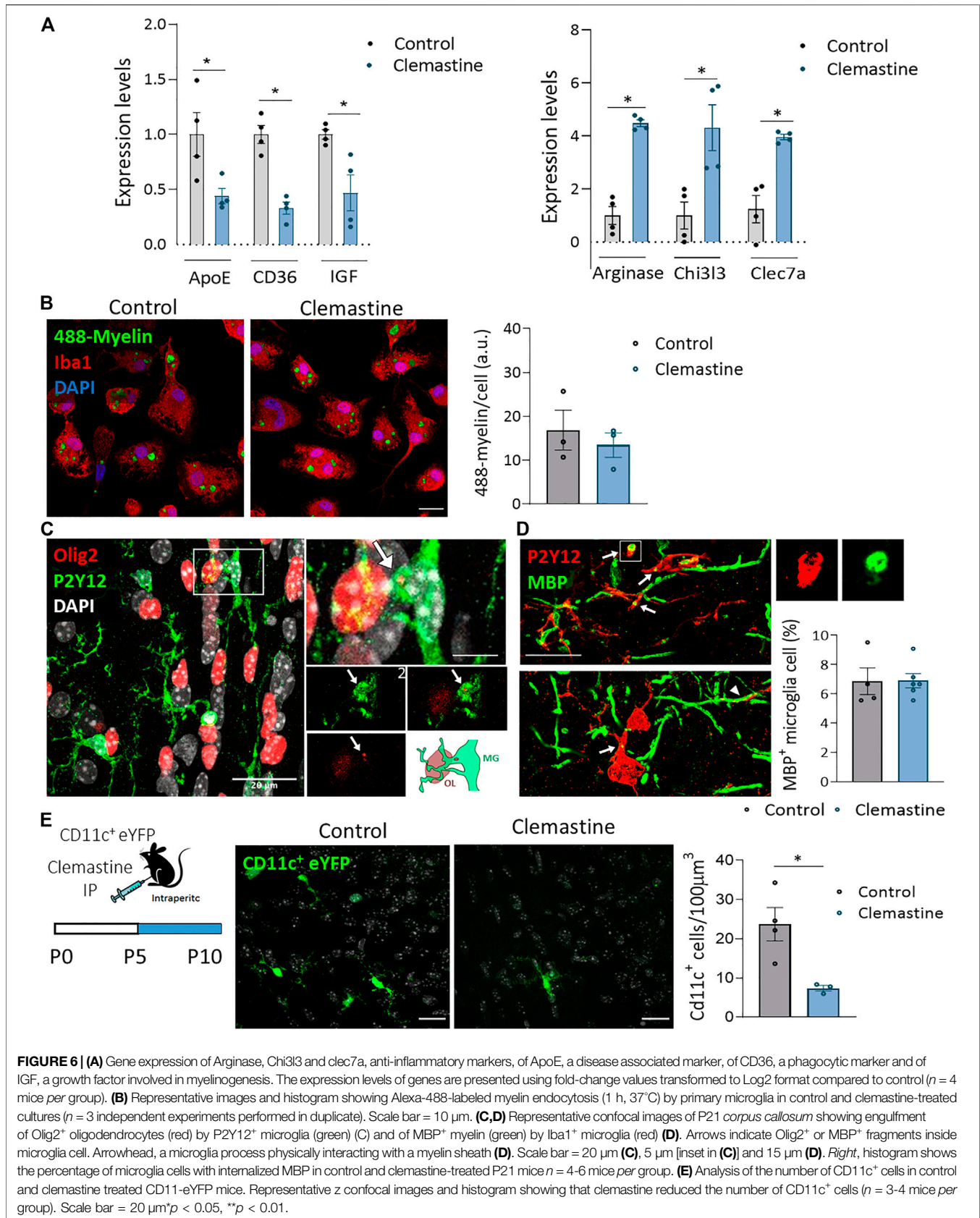
2017) in FACS isolated microglia. Although we did not find changes in pro-inflammatory markers, we observed a significant upregulation of anti-inflammatory markers (**Figure 6A**). In contrast, the expression of ApoE and CD36, genes involved in metabolism and phagocytosis respectively, was significantly downregulated (**Figure 6A**). Microglia removal of myelin debris is determinant for remyelination (Lampron et al., 2015) and its phagocytic efficiency depends on microglia pro/anti-inflammatory activation state (Miron et al., 2013; Zabala et al., 2018). Since myelin pruning have been previously described during development (Hughes and Appel, 2019; Li et al., 2019), we hypothesized that clemastine could indirectly affect developmental myelination by modulating myelin phagocytosis. We next analyzed the impact of clemastine in myelin phagocytosis *in vitro*. For that, myelin was isolated from adult rat whole brain using sucrose gradient (Norton and Poduslo, 1973), labeled with the dye Alexa-488 and added to microglia cultures. We did not detect any effect of clemastine on myelin phagocytosis *in vitro* (**Figure 6B**). We further checked *in vivo* whether clemastine could modulate myelin pruning and/ or OPC phagocytosis, two processes described to refine myelination during development (Hughes and Appel, 2019; Nemes-Baran et al., 2020). We co-immunostained tissue sections from control and clemastine-treated mice at P21 using antibodies to Olig2 or MBP and microglia markers to visualize oligodendroglial cell or myelin engulfment by microglia. We found microglial P2Y12[+] processes frequently contacting Olig2^{+} oligodendroglial cells (large arrowhead in **Figure 6C**) but only very occasionally we observed Olig2^{+} fragments into

microglia (arrow in **Figure 6C**). In turn, we detected more frequently MBP[+] myelin fragments, indicating that microglia phagocytose myelin in normal conditions, as previously described (Hughes and Appel, 2019; Djannatian et al., 2021). We also detected abundant contacts of microglial processes with myelin sheaths (arrowheads in **Figure 6D**). Blinded quantification of microglial cells containing MBP inclusions in 3D confocal images revealed that clemastine treatment *in vivo* did not significantly change the number of MBP[+] microglia in *corpus callosum* (**Figure 6D**). Thus, although myelin phagocytosis by microglia could tune myelination during development, clemastine do not affect this process during development.

Notably, clemastine induced a significant reduction in IGF expression in microglia (**Figure 6A**). Microglia CD11c^{+} has been described as a microglial subset expressed transiently in *corpus callosum* during development that play a pivotal role in myelinogenesis since it is the main source of IGF, a growth factor essential for myelinogenesis. We next analyzed, using CD11c^{+} eYFP reporter mice, the impact of clemastine in this cell type population. Since microglia CD11c^{+} is a transient population that disappears early during development, we treated mice with clemastine from P5 to P10. Blinded analysis showed that clemastine reduced the number of microglia CD11c^{+} in *corpus callosum* in clemastine-treated mice (**Figure 6E**). Altogether, these results are consistent with the hypothesis that clemastine activation of muscarinic receptors in microglia modulate this cell type population leading to an impairment or a delay in myelin development.

FIGURE 5 | (A) Graph showing Chmr1 gen expression in all CNS cell types. Note that Chmr1 is also expressed in microglia. Data was taken from BrainRNA-seq database (Zhang et al., 2014). **(B)** Recordings of Ca^{2+} responses in microglia *in vitro* following application of muscarine (100 μM; arrow) using Fluo-4. Data represent average ±s.e.m. of values obtained from more than 50 cells from 3 different cultures. **(C)** Quantification of the number of Iba1+ microglia cells as well as Iba1 staining intensity in *corpus callosum* of control and clemastine-treated mice. **(D)** Representative skeletonized images of microglia used for morphological analysis. Scale bar = 10 μm. Graphs show average of the number of branches, junctions and sholl analysis of microglia in control and clemastine-treted mice. **(E)** Representative compressed z confocal images showing the expression of iNOS, a pro-inflammatory marker, and CD68, a phagocytic marker, in Iba1$^+$ microglia in *corpus callosum* of control and clemastine-treated mice. Scale bar = 10 μm. Graphs show the average P2y12 and CD68 staining intensity (n = 6 mice *per* group). *p < 0.05, **p < 0.01.

FIGURE 6 | (A) Gene expression of Arginase, Chi3l3 and clec7a, anti-inflammatory markers, of ApoE, a disease associated marker, of CD36, a phagocytic marker and of IGF, a growth factor involved in myelinogenesis. The expression levels of genes are presented using fold-change values transformed to Log2 format compared to control ($n = 4$ mice *per* group). **(B)** Representative images and histogram showing Alexa-488-labeled myelin endocytosis (1 h, 37°C) by primary microglia in control and clemastine-treated cultures ($n = 3$ independent experiments performed in duplicate). Scale bar = 10 μm. **(C,D)** Representative confocal images of P21 *corpus callosum* showing engulfment of Olig2^{+} oligodendrocytes (red) by P2Y12[+] microglia (green) (C) and of MBP[+] myelin (green) by Iba1^{+} microglia (red) **(D)**. Arrows indicate Olig2^{+} or MBP[+] fragments inside microglia cell. Arrowhead, a microglia process physically interacting with a myelin sheath **(D)**. Scale bar = 20 μm **(C)**, 5 μm [inset in **(C)**] and 15 μm **(D)**. *Right*, histogram shows the percentage of microglia cells with internalized MBP in control and clemastine-treated P21 mice n = 4-6 mice *per* group. **(E)** Analysis of the number of CD11c^{+} cells in control and clemastine treated CD11-eYFP mice. Representative z confocal images and histogram showing that clemastine reduced the number of CD11c^{+} cells (n = 3-4 mice *per* group). Scale bar = 20 μm*$p < 0.05$, **$p < 0.01$.

DISCUSSION

Here we report that clemastine treatment during development promotes oligodendrocyte differentiation and alters myelination. In addition, our results also demonstrate that clemastine reduces the density of CD11c + microglial cells, a transient microglia subtype present during development that is involved in myelinogenesis. These findings strongly suggest that clemastine final outcome on myelination may depend on microglia-oligodendrocytes crosstalk.

Clemastine do Not Increase Myelination in Developing Brain, Despite the Increase in Oligodendrocyte Differentiation

Clemastine was identified in a high-throughput study (Mei et al., 2014) as a drug inducing oligodendrocyte progenitor differentiation *in vitro*. The drug facilitates remyelination after demyelination (Li et al., 2015; Mei et al., 2016). Thus, clemastine promotes remyelination in animal models of multiple sclerosis and after ischemic insults (Cree et al., 2018; Wang et al., 2018). Myelin renewal induced by clemastine also prevents cognitive symptoms secondary to aging and Alzheimer's disease (Wang et al., 2020; Chen et al., 2021). Finally, it has been described to promote myelination and to rescue behavioral phenotype in socially isolated mice (Liu et al., 2016). In contrast, no clinical benefit of clemastine was obtained in animal models of Pelizaeus Merzbacher disease (Turski et al., 2018), a dysmyelinating disorder of the central nervous system caused by impaired differentiation of oligodendrocytes during development. In accordance, we found that developmental myelination is not increased after chronic clemastine treatment, even if clemastine induced an increase in oligodendrocyte differentiation. The dose used in our study was similar to those used in other studies (30–50 mg/kg; Turski et al., 2018; Liu et al., 2016). In addition, clemastine crosses the blood brain barrier and reaches the CNS parenchyma, as determined by mass spectrometry (Turski et al., 2018).

Of note, both the study of Tursky and others and ours tested the therapeutical potential of clemastine during development, whereas all the previous studies analyzed the effect of clemastine on adult mice after demyelination or altered myelination. The other important difference is that mice either do not have demyelination (in our study) or have a primary myelination disorder in Pelizaeus Merzbacher disease mice (Turski et al., 2018), whereas in the other models in which clemastine has been tested, myelination deficits were induced by toxins, inflammation or social deprivation and most of the studies are associated with chronic inflammation.

Clemastine Impact on CD11c⁺ Microglia-Oligodendrocyte Crosstalk Could Influence Myelin Development

Although the beneficial effect of clemastine is extended to different insults and diseases, the underlying mechanisms are still unclear. *In vitro* screening proposes muscarinic M1 receptor as the target for the effect in OPCs promoting its maturation (Deshmukh et al., 2013; Mei et al., 2014). Indeed, we observed that mice treated with clemastine during development showed an increase in oligodendrocyte maturation, as revealed by the ratio NG2⁺/APC⁺. However, myelin wrapping of axons seems to be incomplete or delayed in clemastine-treated mice. This result suggests the existence of fine and alternative mechanisms regulating clemastine effect on developmental myelination. In addition to oligodendrocytes, it has been reported that clemastine could interact with microglia too as it possess immune suppressive properties. Indeed, clemastine promotes neuronal protection in animal models of ALS and alleviates hypomyelination after hypoxia by modulating microglia inflammatory reaction (Apolloni et al., 2016; Xie et al., 2021).

Our study also shows that clemastine targets microglia cells during development and induces morphological changes as well as changes in the expression of inflammatory markers, a fact that could indirectly impact developmental myelination. Microglia activation towards an anti-inflammatory phenotype accelerates remyelination by removing myelin debris and by releasing pro-inflammatory factors such as activin, BDNF (Miron et al., 2013; Zabala et al., 2018) but the impact of microglia activation in myelin development have not been sufficiently addressed. Pharmacological suppression of microglia activation with minocycline enhance oligodendrogenesis and reduce OPC differentiation into mature cells (Shigemoto-Mogami et al., 2014). Importantly, microglia in early postnatal white matter are transcriptionally similar to microglia found in disease states, showing elevated expression of pro-inflammatory cytokines and chemokines genes such as *Mif, Ccl3, Ccl4, CCcl6, Ccl9 and Clec7a* (Li et al., 2019). Whether modulation of this particular microglia subset regulates myelin development and whether clemastine impacts on these microglia needs further studies.

On the other hand, a particular CD11c⁺ microglia subset that predominates in primary myelinating areas of the developing brain is essential for myelinogenesis (Wlodarczyk et al., 2017). These cells promote myelinogenesis because they are the major source of insulin-like growth factor (IGF), a factor critical for proper myelin formation (Goebbels et al., 2010; Harrington et al., 2010). The primary signaling receptor, insulin-like growth factor-1 receptor (IGF1R), is a transmembrane tyrosine kinase receptor that binds insulin-like growth factors 1 and 2 (IGF1 and IGF2) and signals through the PI3K-AKT-mTOR, a signaling pathway whose precise regulation is critical for proper myelin formation. IGF modulates lipid metabolism (Hackett et al., 2020), a pathway essential for myelination, not for oligodendrocyte differentiation. Thus, expression of constitutively active Akt in oligodendrocytes and their progenitor cells generated no more oligodendrocytes, but dramatically more myelin, indicating that this signaling pathway could affect myelin generation without affecting OL differentiation (Flores et al., 2008). Similarly, IGF1 overexpressing mice showed a dramatic increase in the amount of myelin *per* oligodendrocyte, but normal numbers of oligodendrocytes (Carson et al., 1993). More recent studies involved the Akt-mTOR signaling pathway in myelin sheath growth (Fedder-Semmes and Appel, 2021). In our study we showed a significant reduction of IGF and of CD11c⁺ microglia cells in the *corpus callosum* of clemastine-treated mice. Interestingly, histamine H1 receptors modulate dendritic cell (also Cd11c⁺ cells) function (Schenk et al., 2016). It could be

possible that clemastine modulates CD11c^{+} microglia response, through muscarinic or histaminic receptors, and blocks the process of myelin wrapping by mature myelinating oligodendrocytes during development.

In addition to the clinical significance for future therapies based on clemastine or others muscarinic antagonists, our data showing that more oligodendrocytes do not lead to more myelin during development suggest the existence of more refined mechanisms to promote a proper myelination and to prevent an excess, probably pathological, of myelin. Indeed, previous data demonstrated that an increase in oligodendrogenesis and myelin supply exceeding axonal demand leads to aberrant myelination of neuronal cell bodies (Almeida et al., 2018). Recent data on literature, as well as data obtained in this study, point to microglia as a key player to modulate myelin organization and prevent aberrant myelination. Blocking live OPC phagocytosis by microglia leads to a thinner myelin (Nemes-Baran et al., 2020). Microglial cells engulf myelin sheaths during development to sculpt myelination according to axonal activity (Hughes & Appel, 2019). Finally, myelin abnormalities arising during development such as outfolding, bulbing, fragmentation and splitting are removed by microglial cells (Djannatian et al., 2021). More studies are needed to understand the microglia-oligodendrocyte crosstalk necessary for myelin health maintenance.

DATA AVAILABILITY STATEMENT

The raw data supporting the conclusion of this article will be made available by the authors, without undue reservation.

ETHICS STATEMENT

The animal study was reviewed and approved by the Ethics Committee of the University of the Basque Country (UPV/EHU).

AUTHOR CONTRIBUTIONS

MD contributed to the conception and design of the study, data interpretation and manuscript writing. AP performed all the experiments, analyzed and interpreted the data and prepared the manuscript. JC contributed to the EM preparation and

analysis. AO-de-A contributed to the histological analysis. AM analyse myelin phagocytosis *in vitro*. FR-J and AP performed treatments on EGFP-CD11c^{+} mice. CM substantially contributed to the revision of the manuscript. AP-S contributed to the electrophysiological study design and analysis, and revised the manuscript. All authors contributed to the manuscript revision, read, and approved the submitted version.

SUPPLEMENTARY MATERIAL

The Supplementary Material for this article can be found online at: https://www.frontiersin.org/articles/10.3389/fcell.2022.841548/full#supplementary-material

Supplementary Figure S1 | (A) Confocal images of proliferating Ki67^{+} (green) Olig2^{+} (red) oligodendrocytes in *corpus callosum* (cc) and retrosplenial cortex (ctx rsp) of control and clemastine-treated mice. Below, average of the percentage of proliferating Ki67^{+} *vs* total Olig2^{+} oligodendroglial cells (*n*= 6 mice *per* experimental group). Scale bar = 50 µm. *p<0,05, **p<0,01. **(B)** Confocal images of Casp-3^{+} (green) Olig2^{+} (red) oligodendrocytes in *corpus callosum* (cc) of control and clemastine-treated mice. Scale bar = 15 µm.

Supplementary Figure S2 | (A) Confocal images of GFAP[+] astrocytes in *corpus callosum* of control and clemastine-treated mice. Scale bar = 50 µm. Below, average GFAP immunoreactivity in *corpus callosum* (cc) and retrospenial cortex (ctx rsp) of control and clemastine-treated mice (*n*= 6 mice *per* group). *p<0.05.

REFERENCES

Almeida, R. G., Pan, S., Cole, K. L. H., Williamson, J. M., Early, J. J., Czopka, T., et al. (2018). Myelination of Neuronal Cell Bodies when Myelin Supply Exceeds Axonal Demand. *Curr. Biol.* 28 (8), 1296–1305. doi:10.1016/j.cub.2018.02.068

Apolloni, S., Fabbrizio, P., Amadio, S., and Volonté, C. (2016). Actions of the Antihistaminergic Clemastine on Presymptomatic SOD1-G93a Mice Ameliorate ALS Disease Progression. *J. Neuroinflammation* 13 (1), 1–15. doi:10.1186/s12974-016-0658-8

Arancibia-Cárcamo, I. L., Ford, M. C., Cossell, L., Ishida, K., Tohyama, K., and Attwell, D. (2017). Node of Ranvier Length as a Potential Regulator of Myelinated Axon Conduction Speed. *ELife* 6, 1–15. doi:10.7554/eLife.23329

Carson, M. J., Behringer, R. R., Brinster, R. L., and McMorris, F. A. (1993). Insulin-like Growth Factor I Increases Brain Growth and central Nervous System Myelination in tTransgenic Mice. *Neuron* 10 (4), 729–740. doi:10.1016/0896-6273(93)90173-O

Chen, J.-F., Liu, K., Hu, B., Li, R.-R., Xin, W., Chen, H., et al. (2021). Enhancing Myelin Renewal Reverses Cognitive Dysfunction in a Murine Model of Alzheimer's Disease. *Neuron* 109 (14), 2292–2307. doi:10.1016/j.neuron.2021.05.012

Cree, B. A. C., Niu, J., Hoi, K. K., Zhao, C., Caganap, S. D., Henry, R. G., et al. (2018). Clemastine Rescues Myelination Defects and Promotes Functional Recovery in Hypoxic Brain Injury. *Brain* 141 (1), 85–98. doi:10.1093/brain/awx312

de Angelis, F., Bernardo, A., Magnaghi, V., Minghetti, L., and Tata, A. M. (2012). Muscarinic Receptor Subtypes as Potential Targets to Modulate Oligodendrocyte Progenitor Survival, Proliferation, and Differentiation. *Devel Neurobio* 72 (5), 713–728. doi:10.1002/dneu.20976

Deshmukh, V. A., Tardif, V., Lyssiotis, C. A., Green, C. C., Kerman, B., Kim, H. J., et al. (2013). A Regenerative Approach to the Treatment of Multiple Sclerosis. *Nature* 502 (7471), 327–332. doi:10.1038/nature12647

Djannatian, M., Weikert, U., Safaiyan, S., Wrede, C., Kislinger, G., Ruhwedel, T., et al. (2021). Myelin Biogenesis Is Associated with Pathological Ultrastructure that Is Resolved by Microglia during Development. *BioRxiv, 2021.02.02.429485*. doi:10.1101/2021.02.02.429485

Domercq, M., Sánchez-Gómez, M. V., Sherwin, C., Etxebarria, E., Fern, R., and Matute, C. (2007). System Xc− and Glutamate Transporter Inhibition Mediates Microglial Toxicity to Oligodendrocytes. *J. Immunol.* 178 (10), 6549–6556. doi:10.4049/jimmunol.178.10.6549

Dutta, D. J., Woo, D. H., Lee, P. R., Pajevic, S., Bukalo, O., Huffman, W. C., et al. (2019). Correction for Dutta et al., Regulation of myelin structure and conduction velocity by perinodal astrocytes. *Proc. Natl. Acad. Sci. USA* 116 (25), 12574. doi:10.1073/pnas.1908361116

Fang, L., Zhao, N., Caudal, L. C., Zhao, R., Lin, C.-H., Chang, H.-F., et al. (2021). Impaired Bidirectional Communication between Interneurons and Oligodendrocyte Precursor Cells Affects Cognitive Behavior. *BioRxiv*. doi:10.1101/2021.05.04.442422

Fedder-Semmes, K. N., and Appel, B. (2021). The Akt-Mtor Pathway Drives Myelin Sheath Growth by Regulating Cap-dependent Translation. *J. Neurosci.* 41 (41), 8532–8544. doi:10.1523/JNEUROSCI.0783-21.2021

Flores, A. I., Narayanan, S. P., Morse, E. N., Shick, H. E., Yin, X., Kidd, G., et al. (2008). Constitutively Active Akt Induces Enhanced Myelination in the CNS. *J. Neurosci.* 28 (28), 7174–7183. doi:10.1523/JNEUROSCI.0150-08.2008

Geraghty, A. C., Gibson, E. M., Ghanem, R. A., Greene, J. J., Ocampo, A., Goldstein, A. K., et al. (2019). Loss of Adaptive Myelination Contributes to Methotrexate Chemotherapy-Related Cognitive Impairment. *Neuron* 103 (2), 250–265. doi:10.1016/j.neuron.2019.04.032

Goebbels, S., Oltrogge, J. H., Kemper, R., Heilmann, I., Bormuth, I., Wolfer, S., et al. (2010). Elevated Phosphatidylinositol 3,4,5-trisphosphate in Glia Triggers Cell-Autonomous Membrane Wrapping and Myelination. *J. Neurosci.* 30 (26), 8953–8964. doi:10.1523/JNEUROSCI.0219-10.2010

Hackett, A. R., Strickland, A., and Milbrandt, J. (2020). Disrupting Insulin Signaling in Schwann Cells Impairs Myelination and Induces a Sensory Neuropathy. *Glia* 68 (5), 963–978. doi:10.1002/glia.23755

Harrington, E. P., Zhao, C., Fancy, S. P. J., Kaing, S., Franklin, R. J. M., and Rowitch, D. H. (2010). Oligodendrocyte PTEN Is Required for Myelin and Axonal Integrity, Not Remyelination. *Ann. Neurol.* 68 (5), 703–716. doi:10.1002/ana.22090

Hughes, A. N., and Appel, B. (2019). Oligodendrocytes Express Synaptic Proteins that Modulate Myelin Sheath Formation. *Nat. Commun.* 10 (1), 4125. doi:10.1038/s41467-019-12059-y

Lampron, A., Larochelle, A., Laflamme, N., Préfontaine, P., Plante, M.-M., Sánchez, M. G., et al. (2015). Inefficient Clearance of Myelin Debris by Microglia Impairs Remyelinating Processes. *J. Exp. Med.* 212 (4), 481–495. doi:10.1084/jem.20141656

Lau, L. W., Cua, R., Keough, M. B., Haylock-Jacobs, S., and Yong, V. W. (2013). Pathophysiology of the Brain Extracellular Matrix: A New Target for Remyelination. *Nat. Rev. Neurosci.* 14 (10), 722–729. doi:10.1038/nrn3550

Li, Q., Cheng, Z., Zhou, L., Darmanis, S., Neff, N. F., Okamoto, J., et al. (2019). Developmental Heterogeneity of Microglia and Brain Myeloid Cells Revealed by Deep Single-Cell RNA Sequencing. *Neuron* 101 (2), 207–223. doi:10.1016/j.neuron.2018.12.006

Li, Z., He, Y., Fan, S., and Sun, B. (2015). Clemastine Rescues Behavioral Changes and Enhances Remyelination in the Cuprizone Mouse Model of Demyelination. *Neurosci. Bull.* 31 (5), 617–625. doi:10.1007/s12264-015-1555-3

Liu, J., Dupree, J. L., Gacias, M., Frawley, R., Sikder, T., Naik, P., et al. (2016). Clemastine Enhances Myelination in the Prefrontal Cortex and Rescues Behavioral Changes in Socially Isolated Mice. *J. Neurosci.* 36 (3), 957–962. doi:10.1523/JNEUROSCI.3608-15.2016

McKenzie, I. A., Ohayon, D., Li, H., Paes de Faria, J., Emery, B., Tohyama, K., et al. (2014). Motor Skill Learning Requires Active central Myelination. *Science* 346 (6207), 318–322. doi:10.1126/science.1254960

Mei, F., Fancy, S. P. J., Shen, Y.-A. A., Niu, J., Zhao, C., Presley, B., et al. (2014). Micropillar Arrays as a High-Throughput Screening Platform for Therapeutics in Multiple Sclerosis. *Nat. Med.* 20 (8), 954–960. doi:10.1038/nm.3618

Mei, F., Lehmann-Horn, K., Shen, Y.-A. A., Rankin, K. A., Stebbins, K. J., Lorrain, D. S., et al. (2016). Accelerated Remyelination during Inflammatory Demyelination Prevents Axonal Loss and Improves Functional Recovery. *ELife* 5, 1–21. doi:10.7554/eLife.18246

Miron, V. E., Boyd, A., Zhao, J.-W., Yuen, T. J., Ruckh, J. M., Shadrach, J. L., et al. (2013). M2 Microglia and Macrophages Drive Oligodendrocyte Differentiation during CNS Remyelination. *Nat. Neurosci.* 16 (9), 1211–1218. doi:10.1038/nn.3469

Nemes-Baran, A. D., White, D. R., and DeSilva, T. M. (2020). Fractalkine-Dependent Microglial Pruning of Viable Oligodendrocyte Progenitor Cells Regulates Myelination. *Cel Rep.* 32 (7), 108047. doi:10.1016/j.celrep.2020.108047

Norton, W. T., and Poduslo, S. E. (1973). Myelination in Rat Brain: Method of Myelin Isolation. *J. Neurochem.* 21 (4), 749–757. doi:10.1111/j.1471-4159.1973.tb07519.x

Phan, B. N., Bohlen, J. F., Davis, B. A., Ye, Z., Chen, H.-Y., Mayfield, B., et al. (2020). A Myelin-Related Transcriptomic Profile Is Shared by Pitt-Hopkins Syndrome Models and Human Autism Spectrum Disorder. *Nat. Neurosci.* 23 (3), 375–385. doi:10.1038/s41593-019-0578-x

Santos, E. N., and Fields, R. D. (2021). Regulation of Myelination by Microglia. *Sci. Adv.* 7 (50). doi:10.1126/sciadv.abk1131

Schenk, H., Neumann, J., and Kloth, C. (2016). Histamine Regulates Murine Primary Dendritic Cell Functions. *Immunopharmacology and Immunotoxicology* 38 (5), 379–384. doi:10.1080/08923973.2016.1214144

Scott, R., Sánchez-Aguilera, A., van Elst, K., Lim, L., Dehorter, N., Bae, S. E., et al. (2019). Loss ofCntnap2Causes Axonal Excitability Deficits, Developmental Delay in Cortical Myelination, and Abnormal Stereotyped Motor Behavior. *Cereb. Cortex* 29 (2), 586–597. doi:10.1093/cercor/bhx341

Shigemoto-Mogami, Y., Hoshikawa, K., Goldman, J. E., Sekino, Y., and Sato, K. (2014). Microglia Enhance Neurogenesis and Oligodendrogenesis in the Early Postnatal Subventricular Zone. *J. Neurosci.* 34 (6), 2231–2243. doi:10.1523/JNEUROSCI.1619-13.2014

Szulzewsky, F., Pelz, A., Feng, X., Synowitz, M., Markovic, D., Langmann, T., et al. (2015). Glioma-associated Microglia/macrophages Display an Expression Profile Different from M1 and M2 Polarization and Highly Express Gpnmb and Spp1. *PLoS ONE* 10 (2), e0116644–27. doi:10.1371/journal.pone.0116644

Turski, C. A., Turski, G. N., Chen, B., Wang, H., Heidari, M., Li, L., et al. (2018). Clemastine Effects in Rat Models of a Myelination Disorder. *Pediatr. Res.* 83 (6), 1200–1206. doi:10.1038/pr.2018.45

Wang, F., Ren, S.-Y., Chen, J.-F., Liu, K., Li, R.-X., Li, Z.-F., et al. (2020). Myelin Degeneration and Diminished Myelin Renewal Contribute to Age-Related Deficits in Memory. *Nat. Neurosci.* 23 (4), 481–486. doi:10.1038/s41593-020-0588-8

Wang, F., Yang, Y.-J., Yang, N., Chen, X.-J., Huang, N.-X., Zhang, J., et al. (2018). Enhancing Oligodendrocyte Myelination Rescues Synaptic Loss and Improves Functional Recovery after Chronic Hypoxia. *Neuron* 99 (4), 689–701. doi:10.1016/j.neuron.2018.07.017

Wlodarczyk, A., Holtman, I. R., Krueger, M., Yogev, N., Bruttger, J., Khoroshi, R., et al. (2017). A Novel Microglial Subset Plays a Key Role in Myelinogenesis in Developing Brain. *Embo J.* 36 (22), 3292–3308. doi:10.15252/embj.201696056

Xie, Y.-Y., Pan, T.-T., Xu, D.-e., Huang, X., Tang, Y., Huang, W., et al. (2021). Clemastine Ameliorates Myelin Deficits via Preventing Senescence of Oligodendrocytes Precursor Cells in Alzheimer's Disease Model Mouse. *Front. Cel Dev. Biol.* 9, 1–13. doi:10.3389/fcell.2021.733945

Yalçın, B., and Monje, M. (2021). Microenvironmental Interactions of Oligodendroglial Cells. *Develop. Cel* 56 (13), 1821–1832. doi:10.1016/j.devcel.2021.06.006

Zabala, A., Vazquez-Villoldo, N., Rissiek, B., Gejo, J., Martin, A., Palomino, A., et al. (2018). P2X4 Receptor Controls Microglia Activation and Favors Remyelination in Autoimmune Encephalitis. *EMBO Mol. Med.* 10 (8), 1–20. doi:10.15252/emmm.201708743

Zhang, Y., Chen, K., Sloan, S. A., Bennett, M. L., Scholze, A. R., O'Keeffe, S., et al. (2014). An RNA-Sequencing Transcriptome and Splicing Database of Glia, Neurons, and Vascular Cells of the Cerebral Cortex. *J. Neurosci.* 34 (36), 11929–11947. doi:10.1523/jneurosci.1860-14.2014